A Hamiltonian-preserving scheme for the Liouville equation of geometrical optics with transmissions and reflections *

Shi Jin † and Xin Wen ‡

Abstract

We construct a class of Hamiltonian-preserving numerical schemes for a Liouville equation of geometrical optics, with transmissions and reflections. This equation arises in the high frequency limit of the linear wave equation, with discontinuous local wave speed. In our previous work [23], we introduced the Hamiltonian-preserving schemes for the same equation when only complete transmissions or reflections occur at the interfaces. These schemes are extended in this paper to the general case of coexistence of both transmission and reflection satisfying the Snell Law of Refraction, with the correct transmission and reflection coefficients. This scheme allows a hyperbolic stability condition, under which positivity, and stabilities in both l^1 and l^∞ norms, are established. Numerical experiments are carried out to study the numerical accuracy.

*Research supported in part by NSF grant No. DMS-0305080, NSFC under the Project 10228101 and the Basic Research Projects of Tsinghua University under the Project JC2002010, and the Institute for Mathematics and its Applications (IMA) under a New Direction Visiting Professorship.

†Department of Mathematics, University of Wisconsin, Madison, WI 53706, USA, and Department of Mathematical Sciences, Tsinghua University, Beijing 100084, P.R. China. Email address: jin@math.wisc.edu.

‡Department of Mathematical Sciences, Tsinghua University, Beijing 100084, P.R. China. Email address: wenx@mail.tsinghua.edu.cn.

[0]draft, May 9, 2005

1 Introduction

In this paper, we construct and study a numerical scheme for the Liouville equation in d-dimension:

$$f_t + H_{\mathbf{v}} \cdot \nabla_{\mathbf{x}} f - H_{\mathbf{x}} \cdot \nabla_{\mathbf{v}} f = 0\,, \quad t > 0, \quad \mathbf{x}, \mathbf{v} \in R^d\,, \tag{1.1}$$

where the Hamiltonian H possesses the form

$$H(\mathbf{x}, \mathbf{v}) = c(\mathbf{x})|\mathbf{v}| = c(\mathbf{x})\sqrt{v_1^2 + v_2^2 + \cdots + v_d^2} \tag{1.2}$$

with $c(\mathbf{x})$ being the local wave speed. $f(t, \mathbf{x}, \mathbf{v})$ is the density distribution of particles depending on position $\mathbf{x}$, time t and the slowness vector $\mathbf{v}$. In this paper we are concerned with the case when $c(\mathbf{x})$ contains *discontinuities* due to different media. This discontinuity will generate an *interface*, and as a consequence waves crossing this interface will undergo transmissions and reflections.

The bicharacteristics of this Liouville equation (1.1) satisfies the Hamiltonian system:

$$\frac{d\mathbf{x}}{dt} = c(\mathbf{x})\frac{\mathbf{v}}{|\mathbf{v}|}\,, \quad \frac{d\mathbf{v}}{dt} = -c_{\mathbf{x}}|\mathbf{v}|\,. \tag{1.3}$$

In classical mechanics the Hamiltonian (1.2) of a particle remains a constant along particle trajectory, when it is being transmitted or reflected by the interface.

This Liouville equation arises in phase space description of geometrical optics. It is the high frequency limit of the wave equation

$$u_{tt} - c(\mathbf{x})^2 \Delta u = 0, \quad t > 0, \quad \mathbf{x} \in R^d\,. \tag{1.4}$$

Recently several phase space based level set methods are based on this equation, see [15, 20, 27]. Semiclassical limit of wave equations with transmissions and reflections at the interfaces were studied in [1, 26, 32]. A Liouville equation based level set method for the wave front, but with only reflection, was introduced in [7].

In our previous work [23] two classes of numerical schemes that are suitable for the Liouville equation (1.1) with a discontinuous local wave speed $c(\mathbf{x})$ are constructed. The designing principle there was to build the behavior of a particle at the interface–either cross over with a changed velocity or be reflected with a negative velocity (or momentum) according to a constant Hamiltonian–into the numerical flux. See also earlier works [29, 22]. These schemes were called *Hamiltonian-preserving schemes*. It gives a selection criterion for a unique solution to the governing equation, which is linearly hyperbolic with singular (discontinuous or measure-valued) coefficients. For a plane wave hitting a interface, it selects the solution that describes the interface condition in geometrical optics governed by **Snell's Law of refraction** when the wave length is much shorter than the width of the interface while both lengths go to zero. However, this is not the only physically relevant possibility to choose a solution across the interface. When the wave length is much

longer than the width of the interface, while both lengths go to zero, the reflection and transmission waves coexist.

This paper is to construct the numerical scheme which is suitable to deal with the case when both transmission and reflection occur at the same time, with computable transmission and reflection coefficients. As in [23], we still use the *Hamiltonian preserving* principle to determine the velocity across the interface. The new contribution of this paper in to incorporate the transmission and reflection coefficients into the numerical flux, in order to treat both transmission and reflection simultaneously. This new, explicit scheme, like those in [22, 23], allows a typical hyperbolic stability condition $\Delta t = O(\Delta x, \Delta v)$, under which we also establish the positivity, and l^1 and l^∞ stability theory for the scheme.

In geometrical optics applications, one has to solve the Liouville equation like (1.1) with *measure-valued* initial data

$$f(0, \mathbf{x}, \mathbf{v}) = \rho_0(\mathbf{x})\delta(\mathbf{v} - \mathbf{u}_0(\mathbf{x}))\,, \tag{1.5}$$

see for example [31, 11, 20]. The solution at later time remains measure-valued (with finite or even infinite number of concentrations-corresponding to *multivalued* solutions in the physical space). Computation of multivalued solutions in geometrical optics and more generally in nonlinear PDEs has been a very active area of research, see [2, 3, 5, 4, 8, 14, 9, 10, 12, 16, 17, 15, 21, 27, 30, 34].

Direct numerical methods(DNM) for the Liouville equation with measure-valued initial data (1.5), which approximating the initial delta function first and then evolving the Liouville equation, could suffer from poor resolution due to the numerical approximation of the initial data as well as numerical dissipation. The level set method proposed in [19, 20] decomposes the density distribution f into the bounded level set functions obeying the same Liouville equation, which greatly enhances the numerical resolution. The moments can be recovered through some numerical delta integrals. Thus one only involves numerically the delta-function at the output time.

However, the extension of this density distribution decomposing approach to the case when both transmission and reflection coexist is not straightforward. In particular, when the number of transmissions and reflections increase in time, so does the number of needed level set functions satisfying 1.1. This difficulty was already pointed out in [7]. In this paper, when dealing with the measure-valued initial data (1.5) we will just use the DNM. This does not offer the same resolution as those in [23]. It remains an open question on how to extend the decomposition idea of [19, 20] to the case when both transmission and reflection coexist.

This paper is organized as follows. In Sections 2, we present the behavior of waves at an interface, which guides the designing of our scheme. We present the scheme in 1d in Section 3 and study its positivity and stability in both l^∞ and l^1 norms. We extend the scheme to the two space dimension in Section 4 in the simple case of interface aligning with the grids and a plane wave. Numerical examples are given in Section 5 to verify the accuracy of the scheme. We make some concluding remarks in Section 6.

2 The behavior of waves at an interface

In geometrical optics, when a wave moves with its density distribution governed by the Liouville equation (1.1), *its Hamiltonian $H = c|\mathbf{v}|$ should be preserved across the interface:*

$$c^+|\mathbf{v}^+| = c^-|\mathbf{v}^-| \tag{2.1}$$

where the superscripts $\pm$ indicates the right and left limits of the quantity at the interface. The wave can be partly reflected and partly transmitted. The condition (2.1) can be used to determine the particle velocity on one side of the interface from its value on the other side. When a plane wave hits an interface, this condition is equivalent to Snell's Law [23] for refraction

$$\frac{\sin\theta_i}{c_-} = \frac{\sin\theta_t}{c_+} \tag{2.2}$$

and the reflection law

$$\theta_r = \theta_i, \tag{2.3}$$

where θ_i, θ_t and θ_r stand for angles of incident, transmitted and reflected waves. See Fig. 2.1. The reflection coefficient is given by [**?**]

$$\alpha^R = \left(\frac{c^+\cos\theta_i - c^-\cos\theta_t}{c^+\cos\theta_i + c^-\cos\theta_t}\right)^2 \tag{2.4}$$

while the transmission coefficient is $\alpha^T = 1 - \alpha^R$. See for example [1, 26, 32].

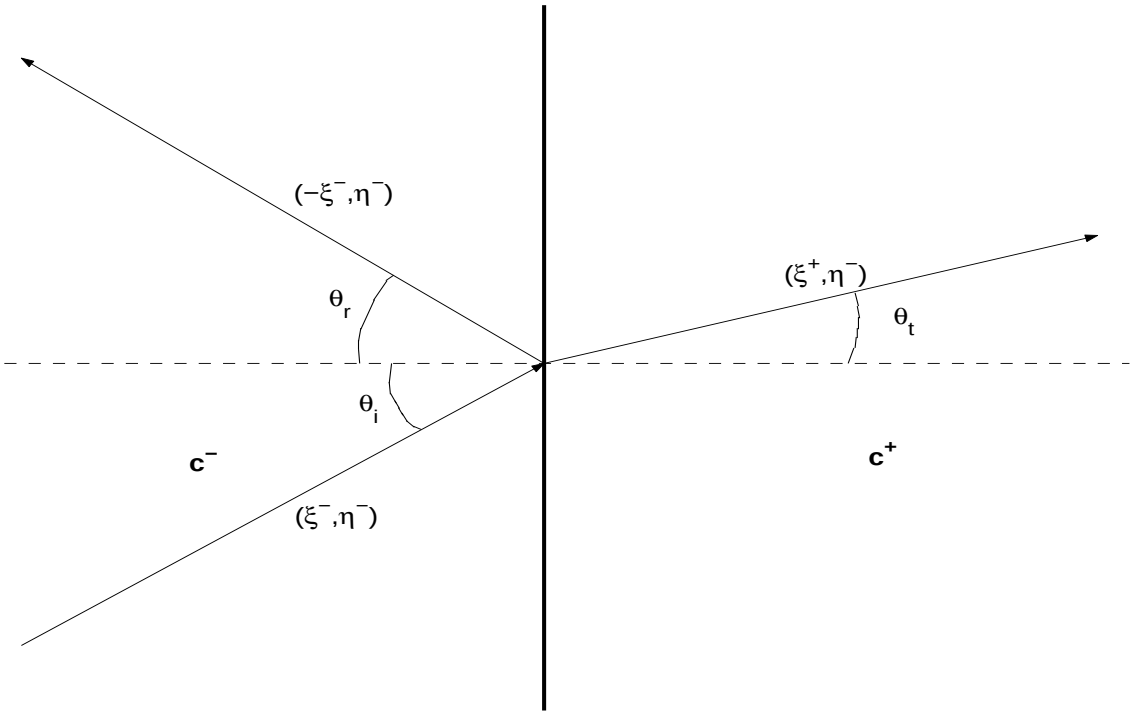

Figure 2.1 Wave transmission and reflection at an interface.

We will discuss this behavior in more details in 1D and 2D respectively.

- The 1D case

  The 1D case is simpler. Consider the case when, at an interface, the characteristic on the left of the interface is given by $\xi^- > 0$. Then with probability $\alpha^R = \left(\dfrac{c^+ - c^-}{c^+ + c^-}\right)^2$ the wave is reflected by the interface with a new velocity $-\xi^-$, and with probability $\alpha^T = 1 - \alpha^R$ it will cross the interface with new velocity $\xi^+ = \dfrac{c^-}{c^+}\xi^-$ determined by (2.1).

- The 2D case, when a plane incident wave hits a vertical interface (see Fig. 2.1).

  Let $\mathbf{x} = (x, y), \mathbf{v} = (\xi, \eta)$. Assume the incident wave has velocity (ξ^-, η^-) to the left side of the interface, with $\xi^- > 0$. Since the interface is vertical (1.3) implies that η is not changed when the wave crosses the interface. There are two possibilities:

  1) $\left(\frac{c^-}{c^+}\right)^2 (\xi^-)^2 + \left[\left(\frac{c^-}{c^+}\right)^2 - 1\right](\eta^-)^2 > 0$. In this case the wave can partially transmit and partially be reflected. With probability $\alpha^R = \left(\dfrac{c^+\gamma^- - c^-\gamma^+}{c^+\gamma^- + c^-\gamma^+}\right)^2$ the wave is reflected with a new velocity $(-\xi^-, \eta^-)$, where

  $$\gamma^+ = \cos(\theta_t) = \frac{\xi^+}{\sqrt{(\xi^+)^2 + (\eta^-)^2}}, \quad \gamma^- = \cos(\theta_i) = \frac{\xi^-}{\sqrt{(\xi^-)^2 + (\eta^-)^2}},$$

  With probability $\alpha^T = 1 - \alpha^R$ it will be transmitted with new velocity (ξ^+, η^-) where

  $$\xi^+ = \sqrt{\left(\frac{c^-}{c^+}\right)^2 (\xi^-)^2 + \left[\left(\frac{c^-}{c^+}\right)^2 - 1\right](\eta^-)^2},$$

  is obtained using (2.1).

  2) $c^- < c^+$ and $\left(\frac{c^-}{c^+}\right)^2 (\xi^-)^2 + \left[\left(\frac{c^-}{c^+}\right)^2 - 1\right](\eta^-)^2 < 0$. In this case, there is no possibility for the wave to transmit, so the wave will be completely reflected with velocity $(-\xi^-, \eta^-)$.

If $\xi^- < 0$, similar behavior can also be analyzed using the constant Hamiltonian condition (2.1).

The solution to the Liouville equation (1.1), which is linearly hyperbolic, can be solved by the method of characteristics. Namely, the density distribution f remains

a constant along a bicharacteristics. However, when transmission and reflection both occur, this is no longer true, since f needs to be determined from two bicharacteristics, one accounting for the transmission and the other for reflection. Therefore, we use the following condition at the interface:

$$f(t, x^+, \xi^+) = \alpha^T f(t, x^-, \xi^-) + \alpha^R f(t, x^+, -\xi^+) \tag{2.5}$$

where ξ^- is defined from ξ^+ through the constant Hamiltonian condition (2.1). This is the main idea in this paper, and will be used in constructing the numerical flux across the interface in the next section.

3 The scheme in one dimension

3.1 The numerical flux

We now describe our finite difference scheme for the 1D Liouville equation

$$f_t + c(x)\text{sign}(\xi) f_x - c_x|\xi| f_\xi = 0\,. \tag{3.1}$$

We employ an uniform mesh with grid points at $x_{i+\frac{1}{2}}, i = 0, \cdots, N$, in the x-direction and $\xi_{j+\frac{1}{2}}, j = 0, \cdots, M$ in the ξ-direction. The cells are centered at $(x_i, \xi_j), i = 1, \cdots, N, j = 1, \cdots, M$ with $x_i = \frac{1}{2}(x_{i+\frac{1}{2}} + x_{i-\frac{1}{2}})$ and $\xi_j = \frac{1}{2}(\xi_{j+\frac{1}{2}} + \xi_{j-\frac{1}{2}})$. The uniform mesh size is denoted by $\Delta x = x_{i+\frac{1}{2}} - x_{i-\frac{1}{2}}, \Delta\xi = \xi_{j+\frac{1}{2}} - \xi_{j-\frac{1}{2}}$. We also assume a uniform time step Δt and the discrete time is given by $0 = t_0 < t_1 < \cdots < t_L = T$. We introduce mesh ratios $\lambda_x^t = \frac{\Delta t}{\Delta x}, \lambda_\xi^t = \frac{\Delta t}{\Delta \xi}$, assumed to be fixed. The cell average of f is defined by

$$f_{ij} = \frac{1}{\Delta x \Delta \xi} \int_{x_{i-\frac{1}{2}}}^{x_{i+\frac{1}{2}}} \int_{\xi_{j-\frac{1}{2}}}^{\xi_{j+\frac{1}{2}}} f(x, \xi, t) d\xi dx.$$

Assume that the discontinuous points of the wave speed c are located at the grid points. Let the left and right limits of $c(x)$ at point $x_{i+1/2}$ be $c^+_{i+\frac{1}{2}}$ and $c^-_{i+\frac{1}{2}}$ respectively. Note that if c is continuous at $x_{j+1/2}$, then $c^+_{i+\frac{1}{2}} = c^-_{i+\frac{1}{2}}$. We approximate c by a piecewise linear function

$$c(x) \approx c^+_{j-1/2} + \frac{c^-_{j+1/2} - c^+_{j-1/2}}{\Delta x}(x - x_{j-1/2})\,.$$

We also define the averaged wave speed as $c_i = \frac{1}{2}(c^+_{i-\frac{1}{2}} + c^-_{i+\frac{1}{2}})$. We will adopt the flux splitting technique used in [29, 22, 23]. The semidiscrete scheme (with time continuous) reads

$$(f_{ij})_t + \frac{c_i \text{sign}(\xi_j)}{\Delta x}(f^-_{i+\frac{1}{2},j} - f^+_{i-\frac{1}{2},j}) - \frac{c^-_{i+\frac{1}{2}} - c^+_{i-\frac{1}{2}}}{\Delta x \Delta \xi}|\xi_j|(f_{i,j+\frac{1}{2}} - f_{i,j-\frac{1}{2}}) = 0, \tag{3.2}$$

where the numerical fluxes $f_{i,j+\frac{1}{2}}$ are defined using the upwind discretization. Since the characteristics of the Liouville equation may be different on the two sides of the interface, the corresponding numerical fluxes should also be different. The essential part of our algorithm is to define the split numerical fluxes $f^-_{i+\frac{1}{2},j}, f^+_{i-\frac{1}{2},j}$ at each cell interface. We will use (2.5) to define these fluxes.

Assume c is discontinuous at $x_{i+\frac{1}{2}}$. Consider the case $\xi_j > 0$. Using upwind scheme, $f^-_{i+\frac{1}{2},j} = f_{ij}$. However,

$$f^+_{i+\frac{1}{2},j} = \alpha^T f(t, x^-_{i+\frac{1}{2}}, \xi^- j) + \alpha^R f(t, x^+_{i+\frac{1}{2}}, -\xi^+)$$

while ξ^- is obtained from $\xi^+_j = \xi_j$ from (2.1). Since ξ^- may not be a grid point, we have to define it approximately. One can first locate the two cell centers that bound this velocity, and then use a linear interpolation to evaluate the needed numerical flux at ξ^-. The case of $\xi_j < 0$ is treated similarly. The detailed algorithm to generate the numerical flux is given below.

Algorithm I

- if $\xi_j > 0$

  $$f^-_{i+\frac{1}{2},j} = f_{ij},$$

  $$\xi' = \frac{c^+_{i+\frac{1}{2}}}{c^-_{i+\frac{1}{2}}}\xi_j$$

  ❑ if $\xi_k \le \xi' < \xi_{k+1}$ for some k

  $$\alpha^R = \left(\frac{c^+_{i+\frac{1}{2}} - c^-_{i+\frac{1}{2}}}{c^+_{i+\frac{1}{2}} + c^-_{i+\frac{1}{2}}}\right)^2, \quad \alpha^T = 1 - \alpha^R$$

  $$f^+_{i+\frac{1}{2},j} = \alpha^T \left(\frac{\xi_{k+1} - \xi'}{\Delta\xi} f_{i,k} + \frac{\xi' - \xi_k}{\Delta\xi} f_{i,k+1}\right) + \alpha^R f_{i+1,k'}$$

  where $\xi_{k'} = -\xi_k$

  ❑ end

- if $\xi_j < 0$

  $$f^+_{i+\frac{1}{2},j} = f_{i+1,j},$$

  $$\xi' = \frac{c^-_{i+\frac{1}{2}}}{c^+_{i+\frac{1}{2}}}\xi_j$$

  ❑ if $\xi_k \le \xi' < \xi_{k+1}$ for some k

  $$\alpha^R = \left(\frac{c^+_{i+\frac{1}{2}} - c^-_{i+\frac{1}{2}}}{c^+_{i+\frac{1}{2}} + c^-_{i+\frac{1}{2}}}\right)^2, \quad \alpha^T = 1 - \alpha^R$$

$$f^-_{i+\frac{1}{2},j} = \alpha^T \left(\frac{\xi_{k+1} - \xi'}{\Delta\xi} f_{i+1,k} + \frac{\xi' - \xi_k}{\Delta\xi} f_{i+1,k+1} \right) + \alpha^R f_{i,k'}$$
where $\xi_{k'} = -\xi_k$

❑ end

The above algorithm for evaluating numerical fluxes is of first order. One can obtain a second order flux by incorporating the slope limiter, such as the van Leer or minmod slope limiter [25], into the above algorithm. This can be achieved by replacing f_{ik} with $f_{ik} + \frac{\Delta x}{2} s_{ik}$, and replacing $f_{i+1,k}$ with $f_{i+1,k} - \frac{\Delta x}{2} s_{i+1,k}$ in the above algorithm for all the possible index k, where s_{ik} is the slope limiter in the x-direction.

After the spatial discretization is specified, one can use any time discretization for the time derivative.

3.2 Positivity and l^∞ contraction

Since the exact solution of the Liouville equation is positive when the initial profile is, it is important that the numerical solution inherits this property.

We only consider the scheme using the first order numerical flux, and the forward Euler method in time. Without loss of generality, we consider the case $\xi_j > 0$ and $c^-_{i+\frac{1}{2}} < c^+_{i-\frac{1}{2}}$ for all i (the other cases can be treated similarly with the same conclusion). The scheme reads

$$\frac{f^{n+1}_{ij} - f^n_{ij}}{\Delta t} + c_i \frac{f_{ij} - (d_1 f_{i-1,k} + d_2 f_{i-1,k+1} + \alpha^R f_{i,k'})}{\Delta x} - \frac{c^-_{i+\frac{1}{2}} - c^+_{i-\frac{1}{2}}}{\Delta x} \xi_j \frac{f_{ij} - f_{i,j-1}}{\Delta\xi} = 0,$$

where d_1, d_2, α^R are non-negative and $d_1 + d_2 = \alpha^T = 1 - \alpha^R$. We omit the superscript n of f. The above scheme can be rewritten as

$$\begin{aligned} f^{n+1}_{ij} &= \left(1 - c_i \lambda^t_x - \frac{\left| c^-_{i+\frac{1}{2}} - c^+_{i-\frac{1}{2}} \right|}{\Delta x} |\xi_j| \lambda^t_\xi \right) f_{ij} + c_i \lambda^t_x \left(d_1 f_{i-1,k} + d_2 f_{i-1,k+1} + \alpha^R f_{i,k'} \right) \\ &+ \frac{\left| c^-_{i+\frac{1}{2}} - c^+_{i-\frac{1}{2}} \right|}{\Delta x} |\xi_j| \lambda^t_\xi f_{i,j-1} \,. \end{aligned} \tag{3.3}$$

Now we investigate the positivity of scheme (3.3). This is to prove that if $f^n_{ij} \geq 0$ for all (i,j), then this is also true for f^{n+1}. Clearly one just needs to show that all the coefficients before f^n are non-negative. A sufficient condition for this is clearly

$$1 - c_i \lambda^t_x - \frac{\left| c^-_{i+\frac{1}{2}} - c^+_{i-\frac{1}{2}} \right|}{\Delta x} |\xi_j| \lambda^t_\xi \geq 0,$$

or

$$\Delta t \max_{i,j} \left[\frac{c_i}{\Delta x} + \frac{\frac{\left| c^-_{i+\frac{1}{2}} - c^+_{i-\frac{1}{2}} \right|}{\Delta x} |\xi_j|}{\Delta\xi} \right] \leq 1. \tag{3.4}$$

The quantity $\frac{\left|c^-_{i+\frac{1}{2}}-c^+_{i-\frac{1}{2}}\right|}{\Delta x}$ now represents the wave speed gradient at its *smooth* point, which has a *finite* upper bound. Thus our scheme allows a time step $\Delta t = O(\Delta x, \Delta t)$.

According to the study in [28], our second order scheme, which incorporates a slope limiter into the first order scheme, is positive under the half CFL condition, namely, the constant on the right hand side of (3.4) is 1/2.

The above conclusion are analyzed based on forward Euler time discretization. One can draw the same conclusion for the second order TVD Runge-Kutta time discretization [33].

The l^∞-contracting property of this scheme:

$$\|f^n\|_\infty \le \|f^0\|_\infty$$

follows easily, because the coefficients in (3.3) are positive and the sum of them is 1.

3.3 The l^1-stability of the scheme

In this section we prove the l^1-stability of the scheme (with the first order numerical flux and the forward Euler method in time). For simplicity, we consider the case when the wave speed has only one discontinuity at grid point $x_{m+\frac{1}{2}}$ with $c^-_{m+\frac{1}{2}} > c^+_{m+\frac{1}{2}}$, and $c'(x) > 0$ at smooth points. The other cases, namely, when $c'(x) \le 0$, or the wave speed having several discontinuity points with increased or decreased jumps, can be discussed similarly. Denote $\lambda_c \equiv c^+_{m+\frac{1}{2}}/c^-_{m+\frac{1}{2}} < 1$.

We consider the general case that $\xi_1 < 0, \xi_M > 0$. For this case, as adopted in [20, 23], the computational domain should exclude a set $O_\xi = \{(x,\xi) \in \mathbb{R}^2 \,|\xi = 0\}$ which causes singularity in the velocity field. For example, we can exclude the following index set

$$D_o = \left\{ (i,j) \middle| |\xi_j| < \frac{\Delta\xi}{2} \right\},$$

from the computational domain.

Since $c(x)$ has a discontinuity, we also define an index set

$$D_l^4 = \{(i,j) | x_i \le x_m, \xi_j < \lambda_c \xi_1\}.$$

Due to the slowness change across at $x = x_{m+\frac{1}{2}}$, D_l^4 represents the area where waves come from outside of the domain $[x_1, x_N] \times [\xi_1, \xi_M]$. In order to implement our scheme conveniently, this index set is also excluded from the computational domain. Thus the computational domain is chosen as

$$E_d = \{(i,j) | i = 1, \cdots, N, j = 1, \cdots, M\} \setminus \left\{ D_o \cup D_l^4 \right\}. \tag{3.5}$$

As a result of excluding the index set D_o from the computational domain, the computational domain is split into two non-overlapping parts

$$E_d = \{(i,j) \in E_d | \xi_j > 0\} \cup \{(i,j) \in E_d | \xi_j < 0\} \equiv E_d^+ \cup E_d^-.$$

We define the l^1-norm of a numerical solution u_{ij} in the set E_d to be

$$|f|_1 = \frac{1}{N_d} \sum_{(i,j)\in E_d} |f_{ij}|$$

with N_d being the number of elements in E_d.

Given the initial data $f_{ij}^0, (i,j) \in E_d$. Denote the numerical solution at time T to be $f_{ij}^L, (i,j) \in E_d$. To prove the l^1-stability, we need to show that $|f^L|_1 \leq C|f^0|_1$.

Due to the linearity of the scheme, the equation for the error between the analytical and the numerical solution is the same as (3.3), so in this section, f_{ij} will denote the error. We assume there is no error at the boundary, thus $f_{ij}^n = 0$ at the boundary. If the l^1-norm of the error introduced at each time step in incoming boundary cells is ensured to be $o(1)$ part of $|f^n|_1$, our following analysis still applies.

Now denote

$$A_i = \frac{1}{\Delta x} \left| c^-_{i+\frac{1}{2}} - c^+_{i-\frac{1}{2}} \right|. \tag{3.6}$$

Assume there exists an $A_u > 0$, such that $A_i < A_u, \forall i$. Assume also that there is an $C_m > 0$ such that C_m, $c_i > C_m, \forall i$. The finite difference scheme is given by

- When $\xi_j > 0$

  1) if $i \neq m+1$,

$$f_{ij}^{n+1} = \left(1 - A_i|\xi_j|\lambda_\xi^t - c_i\lambda_x^t\right) f_{ij} + A_i|\xi_j|\lambda_\xi^t f_{i,j+1} + c_i\lambda_x^t f_{i-1,j}, \tag{3.7}$$

  2)

$$\begin{aligned} f_{m+1,j}^{n+1} &= \left(1 - A_{m+1}|\xi_j|\lambda_\xi^t - c_{m+1}\lambda_x^t\right) f_{m+1,j} + A_{m+1}|\xi_j|\lambda_\xi^t f_{m+1,j+1} \\ &+ c_{m+1}\lambda_x^t(d_{j1}f_{m,k} + d_{j2}f_{m,k+1} + \alpha^R f_{m+1,k'}), \end{aligned} \tag{3.8}$$

- When $\xi_j < 0$

  3) if $i \neq m$,

$$f_{ij}^{n+1} = \left(1 - A_i|\xi_j|\lambda_\xi^t - c_i\lambda_x^t\right) f_{ij} + A_i|\xi_j|\lambda_\xi^t f_{i,j+1} + c_i\lambda_x^t f_{i+1,j}, \tag{3.9}$$

  4)

$$\begin{aligned} f_{mj}^{n+1} &= \left(1 - A_m|\xi_j|\lambda_\xi^t - c_m\lambda_x^t\right) f_{mj} + A_m|\xi_j|\lambda_\xi^t f_{m,j+1} \\ &+ c_m\lambda_x^t(d_{j1}f_{m+1,k} + d_{j2}f_{m+1,k+1} + \alpha^R f_{m,k'}), \end{aligned} \tag{3.10}$$

where $0 \le d_{j1}, d_{j2} \le 1$ and $d_{j1} + d_{j2} = \alpha^T = 1 - \alpha^R = 1$. In (3.8) k is determined by $\xi_k \le \lambda_c \xi_j < \xi_{k+1}$ and $\xi_{k'} = -\xi_k$. In (3.10) k is determined by $\xi_k \le \frac{\xi_j}{\lambda_c} < \xi_{k+1}$ and $\xi_{k'} = -\xi_k$.

When summing up all absolute values of f_{ij}^{n+1} in (3.7)-(3.10), one typically gets the following inequality

$$|f^{n+1}|_1 \le \frac{1}{N_d} \sum_{(i,j)\in E_d} \alpha_{ij} |f_{ij}^n|, \tag{3.11}$$

where the coefficients α_{ij} are positive. One can check that, under the CFL condition (3.4), $\alpha_{ij} \le 1$ except for possibly $(i,j) \in D_{m+1}^- \bigcup D_m^+$, where

$$D_{m+1}^- = \{(i,j) \in E_d^- | i = m+1\}, \quad D_m^+ = \{(i,j) \in E_d^+ | i = m\}.$$

We next derive the bounds for M^-, M^+ defined as

$$M^- = \max_{(m+1,j)\in D_{m+1}^-} \alpha_{m+1,j}, \quad M^+ = \max_{(m,j)\in D_m^+} \alpha_{m,j}.$$

Define the set

$$S_j^{m+1} = \left\{ j' \middle| \xi_{j'} < 0, \left| \frac{\xi_{j'}}{\lambda_c} - \xi_j \right| < \Delta\xi \right\} \quad \text{for } (m+1,j) \in D_{m+1}^-.$$

Let the number of elements in S_j^{m+1} be N_j^{m+1}. One can check that $N_j^{m+1} \le 2\lambda_c + 1$ because every two elements $j_1', j_2' \in S_j^{m+1}$ satisfy $\left| \frac{\xi_{j_1'}}{\lambda_c} - \frac{\xi_{j_2'}}{\lambda_c} \right| \ge \frac{\Delta\xi}{\lambda_c}$.

On the other hand, one can easily check from (3.8) and (3.10), for $(m+1,j) \in D_{m+1}^-$,

$$\alpha_{m+1,j} < 1 - c_{m+1}\lambda_x^t + c_m \lambda_x^t (2\lambda_c + 1)\alpha^T + \alpha^R c_{m+1}\lambda_x^t = 1 + \alpha^T (c_m + c_{m+1})\lambda_x^t + O(\Delta x),$$

so for sufficiently small Δx, M^- can be bounded by

$$M^- < 1 + 2\alpha^T (c_m + c_{m+1})\lambda_x^t.$$

Similarly, one can prove for sufficiently small Δx, M^+ is also bounded by

$$M^+ < 1 + 2\alpha^T (c_m + c_{m+1})\lambda_x^t.$$

Denote $M' = 2\alpha^T (c_m + c_{m+1})\lambda_x^t$. From (3.11),

$$|f^{n+1}|_1 < |f^n|_1 + \frac{M'}{N_d} \sum_{(m+1,j)\in D_{m+1}^-} |f_{m+1,j}^n| + \frac{M'}{N_d} \sum_{(m,j)\in D_m^+} |f_{m,j}^n|. \tag{3.12}$$

Consecutively using (3.12) gives

$$|f^L|_1 < |f^0|_1 + \frac{M'}{N_d}\sum_{n=0}^{L-1}\left\{\sum_{(m+1,j)\in D^-_{m+1}}|f^n_{m+1,j}|\right\} + \frac{M'}{N_d}\sum_{n=0}^{L-1}\left\{\sum_{(m,j)\in D^+_m}|f^n_{m,j}|\right\}. \quad (3.13)$$

Define

$$S_1 = \sum_{n=0}^{L-1}\left\{\sum_{(m+1,j)\in D^-_{m+1}}|f^n_{m+1,j}|\right\}, \quad S_2 = \sum_{n=0}^{L-1}\left\{\sum_{(m,j)\in D^+_m}|f^n_{m,j}|\right\}. \quad (3.14)$$

These two terms can be proved in the same way as in [23] that

$$S_1, S_2 < C_T N_d |f^0|_1, \quad (3.15)$$

where

$$C_T \equiv \exp\left(\frac{2A_u}{C_m}(x_N - x_1)\right)\frac{1}{C_m\lambda^t_x}. \quad (3.16)$$

Combing (3.13) and (3.15),

$$\begin{aligned} |f^L|_1 &< |f^0|_1 + 2C_T M'|f^0|_1 \\ &= [1 + 2C_T M']\,|f^0|_1 \\ &\equiv C|f^0|_1 \end{aligned}$$

where $C \equiv 1 + 2C_T M'$.

Thus we have proved the following theorem

Theorem 3.1. *Under the hyperbolic CFL condition (3.4), the scheme (3.7)-(3.10) is l^1-stable:*

$$|f^L|_1 < C|f^0|_1 .$$

4 The scheme in two space dimension

Consider the 2D Liouville equation

$$f_t + \frac{c(x,y)\xi}{\sqrt{\xi^2+\eta^2}}f_x + \frac{c(x,y)\eta}{\sqrt{\xi^2+\eta^2}}f_y - c_x\sqrt{\xi^2+\eta^2}f_\xi - c_y\sqrt{\xi^2+\eta^2}f_\eta = 0. \quad (4.1)$$

We employ an uniform mesh with grid points at $x_{i+\frac{1}{2}}, y_{j+\frac{1}{2}}, \xi_{k+\frac{1}{2}}, \eta_{l+\frac{1}{2}}$ in each direction. The cells are centered at $(x_i, y_j, \xi_k, \eta_l)$ with $x_i = \frac{1}{2}(x_{i+\frac{1}{2}} + x_{i-\frac{1}{2}}), y_j = \frac{1}{2}(y_{j+\frac{1}{2}} + y_{j-\frac{1}{2}}), \xi_k = \frac{1}{2}(\xi_{k+\frac{1}{2}} + \xi_{k-\frac{1}{2}}), \eta_l = \frac{1}{2}(\eta_{l+\frac{1}{2}} + \eta_{l-\frac{1}{2}})$. The mesh size is denoted

by $\Delta x = x_{i+\frac{1}{2}} - x_{i-\frac{1}{2}}, \Delta y = y_{j+\frac{1}{2}} - y_{j-\frac{1}{2}}, \Delta\xi = \xi_{k+\frac{1}{2}} - \xi_{k-\frac{1}{2}}, \Delta\eta = \eta_{l+\frac{1}{2}} - \eta_{l-\frac{1}{2}}$. We define the cell average of f as

$$f_{ijkl} = \frac{1}{\Delta x\Delta y\Delta\xi\Delta\eta}\int_{x_{i-\frac{1}{2}}}^{x_{i+\frac{1}{2}}}\int_{y_{j-\frac{1}{2}}}^{y_{j+\frac{1}{2}}}\int_{\xi_{k-\frac{1}{2}}}^{\xi_{k+\frac{1}{2}}}\int_{\eta_{l-\frac{1}{2}}}^{\eta_{l+\frac{1}{2}}} f(x,y,\xi,\eta,t)d\eta d\xi dy dx.$$

Similar to the 1D case, we approximate $c(x,y)$ by a piecewise bilinear function, and for convenience, we always provide two interface values of c at each cell interface. When c is smooth at a cell interface, the two potential interface values are identical. We also define the averaged wave speed in a cell by averaging the four cell interface wave speed values

$$c_{ij} = \frac{1}{4}(c^+_{i-\frac{1}{2},j} + c^-_{i+\frac{1}{2},j} + c^+_{i,j-\frac{1}{2}} + c^-_{i,j+\frac{1}{2}}).$$

The 2D Liouville equation (4.1) can be semi-discretized as

$$\begin{aligned}
(f_{ijkl})_t &+ \frac{c_{ij}\xi_k}{\Delta x\sqrt{\xi_k^2+\eta_l^2}}\left(f^-_{i+\frac{1}{2},jkl} - f^+_{i-\frac{1}{2},jkl}\right)\\
&+ \frac{c_{ij}\eta_l}{\Delta y\sqrt{\xi_k^2+\eta_l^2}}\left(f^-_{i,j+\frac{1}{2},kl} - f^+_{i,j-\frac{1}{2},kl}\right)\\
&- \frac{c^-_{i+\frac{1}{2},j} - c^+_{i-\frac{1}{2},j}}{\Delta x\Delta\xi}\sqrt{\xi_k^2+\eta_l^2}\left(f_{ij,k+\frac{1}{2},l} - f_{ij,k-\frac{1}{2},l}\right)\\
&- \frac{c^-_{i,j+\frac{1}{2}} - c^+_{i,j-\frac{1}{2}}}{\Delta y\Delta\eta}\sqrt{\xi_k^2+\eta_l^2}\left(f_{ijk,l+\frac{1}{2}} - f_{ijk,l-\frac{1}{2}}\right)\\
&= 0,
\end{aligned}$$

where the interface values $f_{ij,k+\frac{1}{2},l}, f_{ijk,l+\frac{1}{2}}$ are provided by the upwind approximation, and the split interface values $f^-_{i+\frac{1}{2},jkl}, f^+_{i-\frac{1}{2},jkl}, f^-_{i,j+\frac{1}{2},kl}, f^+_{i,j-\frac{1}{2},kl}$ should be obtained using similar but slightly different algorithm for the 1D case. For example, to evaluate $f^\pm_{i+\frac{1}{2},jkl}$ we can extend Algorithm I as

Algorithm I in 2D

- if $\xi_k > 0$

$$f^-_{i+\frac{1}{2},jkl} = f_{ijkl}, \quad \xi_{k_1} = -\xi_k$$

☆ if $\left(\frac{C^+_{i+\frac{1}{2},j}}{C^-_{i+\frac{1}{2},j}}\right)^2(\xi_k)^2 + \left[\left(\frac{C^+_{i+\frac{1}{2},j}}{C^-_{i+\frac{1}{2},j}}\right)^2 - 1\right](\eta_l)^2 > 0$

$$\xi^- = \sqrt{\left(\frac{C^+_{i+\frac{1}{2},j}}{C^-_{i+\frac{1}{2},j}}\right)^2(\xi_k)^2 + \left[\left(\frac{C^+_{i+\frac{1}{2},j}}{C^-_{i+\frac{1}{2},j}}\right)^2 - 1\right](\eta_l)^2}$$

❏ if $\xi_{k'} \le \xi^- < \xi_{k'+1}$ for some k'

$$\gamma^+ = \frac{\xi_k}{\sqrt{(\xi_k)^2 + (\eta_l)^2}}, \quad \gamma^- = \frac{\xi^-}{\sqrt{(\xi')^2 + (\eta_l)^2}}$$

$$\alpha^R = \left(\frac{c^+_{i+\frac{1}{2}}\gamma^- - c^-_{i+\frac{1}{2}}\gamma^+}{c^+_{i+\frac{1}{2}}\gamma^- + c^-_{i+\frac{1}{2}}\gamma^+} \right)^2, \quad \alpha^T = 1 - \alpha^R$$

$$f^+_{i+\frac{1}{2},jkl} = \alpha^T \left(\frac{\xi_{k'+1} - \xi^-}{\Delta\xi} f_{ij,k',l} + \frac{\xi^- - \xi_{k'}}{\Delta\xi} f_{ij,k'+1,l} \right) + \alpha^R f_{i+1,j,k_1,l}$$

❏ end

✯ else

$$f^+_{i+\frac{1}{2},jkl} = f_{i+1,j,k_1,l}$$

✯ end

- if $\xi_k < 0$

$$f^+_{i+\frac{1}{2},jkl} = f_{i+1,jkl}, \quad \xi_{k_1} = -\xi_k$$

✯ if $\left(\frac{C^-_{i+\frac{1}{2},j}}{C^+_{i+\frac{1}{2},j}} \right)^2 (\xi_k)^2 + \left[\left(\frac{C^-_{i+\frac{1}{2},j}}{C^+_{i+\frac{1}{2},j}} \right)^2 - 1 \right] (\eta_l)^2 > 0$

$$\xi^+ = -\sqrt{\left(\frac{C^-_{i+\frac{1}{2},j}}{C^+_{i+\frac{1}{2},j}} \right)^2 (\xi_k)^2 + \left[\left(\frac{C^-_{i+\frac{1}{2},j}}{C^+_{i+\frac{1}{2},j}} \right)^2 - 1 \right] (\eta_l)^2}$$

❏ if $\xi_{k'} \le \xi^+ < \xi_{k'+1}$ for some k'

$$\gamma^+ = \frac{|\xi^+|}{\sqrt{(\xi^+)^2 + (\eta_l)^2}}, \quad \gamma^- = \frac{|\xi_k|}{\sqrt{(\xi_k)^2 + (\eta_l)^2}}$$

$$\alpha^R = \left(\frac{c^+_{i+\frac{1}{2}}\gamma^- - c^-_{i+\frac{1}{2}}\gamma^+}{c^+_{i+\frac{1}{2}}\gamma^- + c^-_{i+\frac{1}{2}}\gamma^+} \right)^2, \quad \alpha^T = 1 - \alpha^R$$

$$f^-_{i+\frac{1}{2},jkl} = \alpha^T \left(\frac{\xi_{k'+1} - \xi^+}{\Delta\xi} f_{i+1,j,k',l} + \frac{\xi^+ - \xi_{k'}}{\Delta\xi} f_{i+1,j,k'+1,l} \right) + \alpha^R f_{ij,k_1,l}$$

❏ end

✯ else

$$f^-_{i+\frac{1}{2},jkl} = f_{i,j,k_1,l} \text{ where } \xi_{k_1} = -\xi_k$$

✯ end

The flux $f^\pm_{i,j+\frac{1}{2},kl}$ can be constructed similarly.

As introduced in section 2, the essential difference between 1D and 2D split flux definition is that in 2D case, the phenomenon that a wave is completely reflected at

the interface does occur. While in 1D, the transmission and reflection waves always coexist at the interface.

Since the gradient of the wave speed at its smooth points are bounded, this scheme similar to the 1D scheme, is also subject to a hyperbolic CFL condition under which the scheme is positive.

5 Numerical examples

In this section we present numerical examples to demonstrate the validity of the proposed scheme and to study the numerical accuracy. In the numerical computations the second order TVD Runge-Kutta time discretization [33] is used.

Example 5.1. A 1D problem with the exact L^∞-solution. Consider the 1D Liouville equation

$$f_t + c(x)\text{sign}(\xi) f_x - c_x|\xi| f_\xi = 0 \tag{5.1}$$

with a discontinuous wave speed given by

$$c(x) = \begin{cases} 0.6 & x < 0 \\ 0.2 & x > 0 \end{cases}.$$

The initial data is given by

$$f(x,\xi,0) = \begin{cases} 1 & x < 0, \xi > 0, \sqrt{x^2 + 4\xi^2} < 1, \\ 1 & x > 0, \xi < 0, \sqrt{x^2 + \xi^2} < 1, \\ 0 & \text{otherwise}, \end{cases} \tag{5.2}$$

In this example the physically relevant values for the reflection and transmission coefficients α^R, α^T at the interface are $\alpha^R = \frac{1}{4}, \alpha^T = \frac{3}{4}$. The exact phase space solution at $t = 1$ is given by

$$f(x,\xi,1) = \begin{cases} \alpha^T & 0 < x < 0.2, \quad \sqrt{1-(0.2-x)^2} < \xi < 1.5\sqrt{1-(3x-0.6)^2}; \\ 1 & 0 < x < 0.2, \quad 0 < \xi < \sqrt{1-(0.2-x)^2}; \\ 1 & 0 < x < 0.8, \quad -\sqrt{1-(x+0.2)^2} < \xi < 0; \\ 1 & -0.4 < x < 0, \quad 0 < \xi < \frac{1}{2}\sqrt{1-(x-0.6)^2}; \\ 1 & -0.6 < x < 0, \quad -\frac{1}{3}\sqrt{1-(\frac{x}{3}+0.2)^2} < \xi < 0; \\ \alpha^R & -0.6 < x < 0, \quad -\frac{1}{2}\sqrt{1-(x+0.6)^2} < \xi < -\frac{1}{3}\sqrt{1-(\frac{x}{3}+0.2)^2}; \\ 0 & \text{otherwise}, \end{cases} \tag{5.3}$$

as shown in Figure 5.1.

We are also interested in computing the moments of the phase space solution, which is the density

$$\rho(x,t) = \int f(x,\xi,t)d\xi$$

and the averaged slowness

$$u(x,t) = \int f(x,\xi,t)\xi d\xi \Big/ \rho(x,t).$$

At $t = 1$, the exact density is

$$\rho(x,1) = \begin{cases} \sqrt{1-(x+0.2)^2} & 0.2 < x < 0.8; \\ 1.5\alpha^T\sqrt{1-(3x-0.6)^2} + \alpha^R\sqrt{1-(0.2-x)^2} & \\ +\sqrt{1-(x+0.2)^2} & 0 < x < 0.2; \\ \dfrac{\alpha^T}{3}\sqrt{1-(\dfrac{x}{3}+0.2)^2} + \dfrac{\alpha^R}{2}\sqrt{1-(x+0.6)^2} & -0.6 < x < -0.4; \\ \dfrac{\alpha^T}{3}\sqrt{1-(\dfrac{x}{3}+0.2)^2} + \dfrac{\alpha^R}{2}\sqrt{1-(x+0.6)^2} & \\ +\dfrac{1}{2}\sqrt{1-(x-0.6)^2} & -0.4 < x < 0, \\ 0 & \text{otherwise} \end{cases} \tag{5.4}$$

and in the interval $[-0.6, 0.8]$, the exact averaged slowness is

$$u(x,1) = \frac{1}{2\rho(x,1)} \begin{cases} -\left[1-(x+0.2)^2\right] & 0.2 < x < 0.8; \\ 2.25\alpha^T\left[1-(3x-0.6)^2\right] + \alpha^R\left[1-(0.2-x)^2\right] & \\ -\left[1-(x+0.2)^2\right] & 0 < x < 0.2; \\ \dfrac{-\alpha^T}{9}\left[1-(\dfrac{x}{3}+0.2)^2\right] - \dfrac{\alpha^R}{4}\left[1-(x+0.6)^2\right] & -0.6 < x < -0.4; \\ \dfrac{-\alpha^T}{9}\left[1-(\dfrac{x}{3}+0.2)^2\right] - \dfrac{\alpha^R}{4}\left[1-(x+0.6)^2\right] & \\ +\dfrac{1}{4}\left[1-(x-0.6)^2\right] & -0.4 < x < 0. \end{cases} \tag{5.5}$$

We choose the time step as $\Delta t = \frac{1}{2}\Delta\xi$. The computational domain is chosen as $[x,\xi] \in [-1.5, 1.5] \times [-1.6, 1.6]$. Table 5.1 compares the l^1-error of the numerical solutions for f, rho on $[-1.5, 1.5]$ and u on $[-0.6, 0.8]$ computed with different meshes respectively.

The convergence rate of the numerical phase space solution in l^1-norm is shown to be about 0.74. This agrees with the well established theory [24], [35], that the l^1-error by finite difference scheme for a discontinuous solution of a linear hyperbolic equation is at most half order. The convergence rate of the numerical density and averaged slowness are shown to be about 0.74 and 0.98 respectively since the solutions also contain discontinuities away from the interface.

Figure 5.2 shows the numerical density ρ and averaged slowness u computed with a 400× 400 cell along with the exact solutions in the physical space.

Table 5.1 l^1 error of the numerical solutions with different meshes

grid points	50 × 50	100 × 100	200× 200	400× 400
f	0.179090	0.104788	0.064989	0.038535
ρ	0.124361	0.079007	0.043248	0.025187
u	0.143083	0.063068	0.043079	0.019870

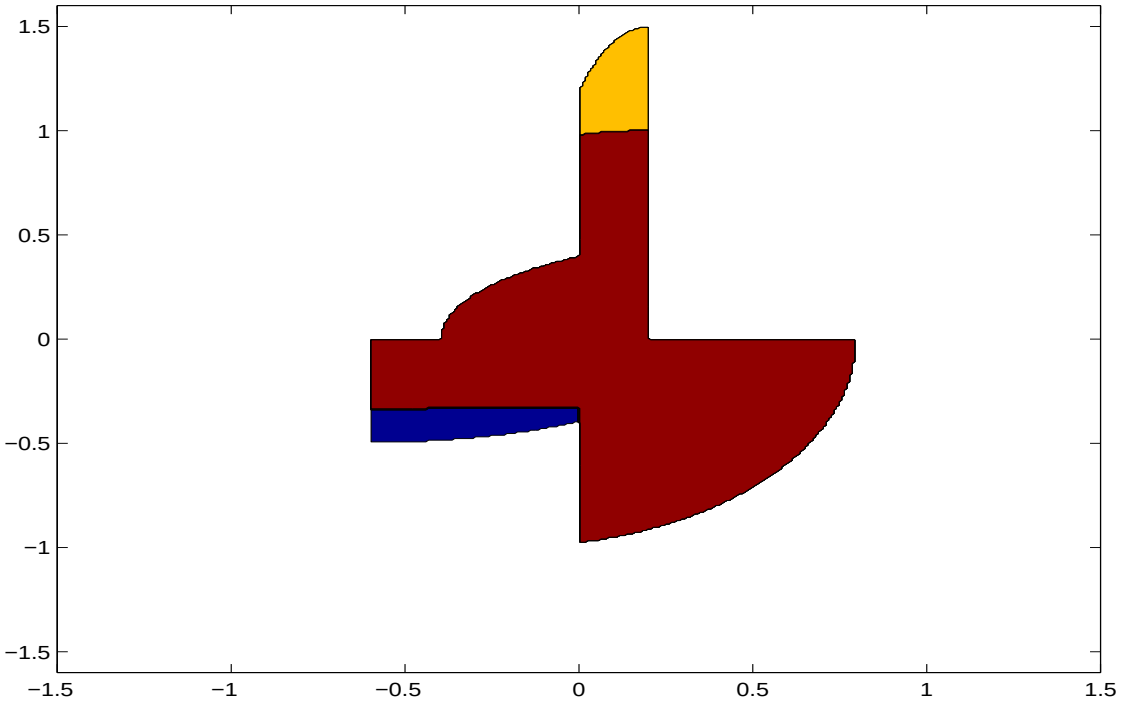

Figure 5.1 Example 5.1, the non-zero part of the exact solution $f(x, \xi, 1)$ depicted on the 400 × 400 mesh. The horizontal axis is the position, the vertical axis is the slowness.

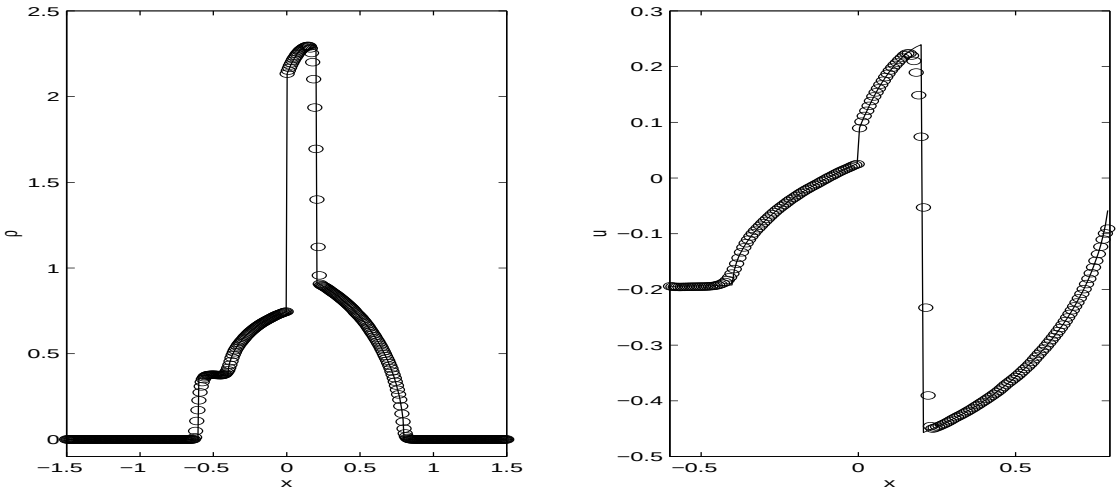

Figure 5.2 Example 5.1, the density ρ and averaged slowness u at $t = 1$. Solid line: the exact solution; 'o': the numerical solutions using the 400×400 mesh. Left: the density ρ ; Right: the averaged slowness u.

Example 5.2. Computing the physical observables of a 1D problem with measure-valued solution. Consider the 1D Liouville equation (5.1), where the wave speed is a well-shaped function

$$c(x) = \begin{cases} 0.6 & -0.4 < x < 0.4 \\ 1 & \text{else} \end{cases}$$

and the initial data is a delta-function

$$f(x, \xi, 0) = \delta(\xi - w(x)) \tag{5.6}$$

with

$$w(x) = \begin{cases} 0.5, & x \le -1.6; \\ 0.5 - \dfrac{0.4}{(1.6)^2}(x + 1.6)^2, & -1.6 < x \le 0; \\ -0.5 + \dfrac{0.4}{(1.6)^2}(x - 1.6)^2, & 0 < x < 1.6; \\ -0.5, & x \ge 1.6\,. \end{cases} \tag{5.7}$$

Figure 5.3 plots $w(x)$ in dashed lines.

In this example we are interested in the approximation of the density

$$\rho(x, t) = \int f(x, \xi, t) d\xi\,,$$

and the averaged slowness

$$u(x, t) = \frac{\int f(x, \xi, t)\xi d\xi}{\int f(x, \xi, t) d\xi}\,.$$

In the computation, we first approximate the delta function initial data (5.6) by a discrete delta function [13]:

$$\delta_w(x) = \begin{cases} \frac{1}{w}\left(1 - |\frac{x}{w}|\right), & |\frac{x}{w}| \le 1 \\ 0, & |\frac{x}{w}| > 1 \end{cases} \tag{5.8}$$

with $w = \Delta\xi$ to regularize the initial data (5.6). If $|\xi_j - w(x_i)| < \Delta\xi$, set $f_{ij}^0 = \frac{1}{\Delta\xi}\left(1 - |\frac{\xi_j - w(x_i)}{\Delta\xi}|\right)$, and $f_{ij}^0 = 0$ otherwise. We then use the first order Hamiltonian preserving scheme (without slope limiter) to calculate the phase space solution of Liouville equation (5.1) (we noticed a nonconvergence phenomenon for such problems with measure -valued initial data when using second order shock capturing upwind methods with slope limiters, which is still under investigation). Then the moments are recovered by

$$\rho_i^n = \sum_j f_{ij}^n \Delta\xi, \quad u_i^n = \left(\sum_j f_{ij}^n \xi_j \Delta\xi\right) \Big/ \rho_i^n.$$

When both transmission and reflection happen at wave speed jump, the exact multi-valued slowness at $t = 1$ is depicted as the solid line in Figure 5.3.

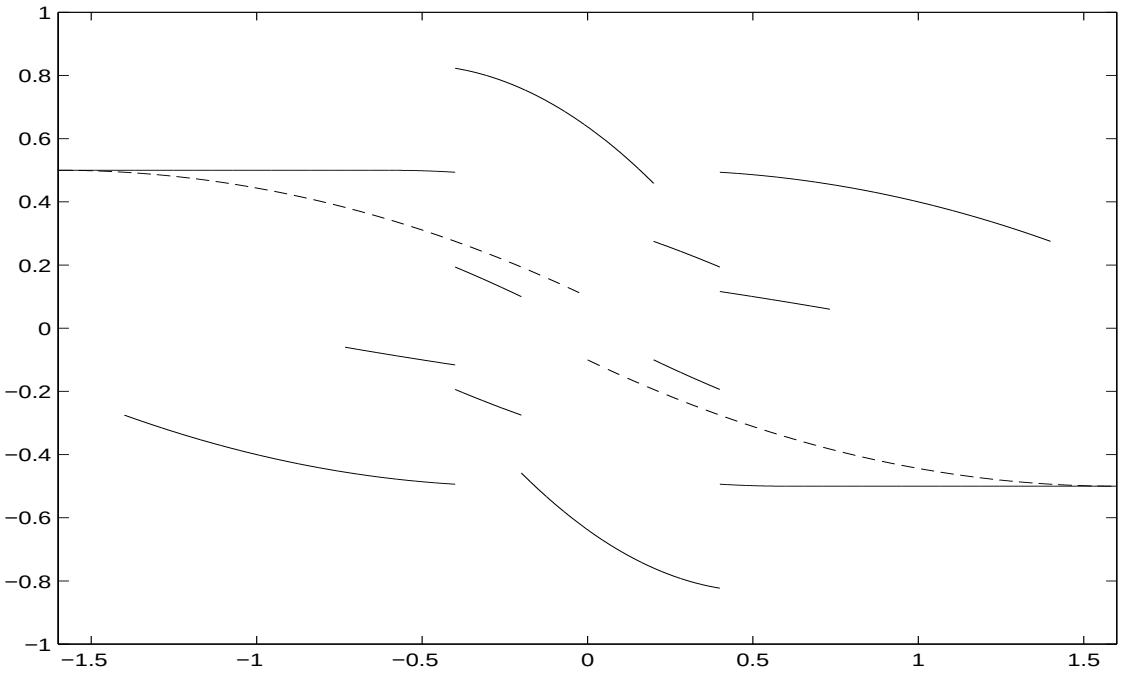

Figure 5.3 Example 5.2, slowness. Dashed line: the initial slowness $w(x)$; Solid line: the slowness at $t = 1$. The horizontal axis is the position, the vertical axis is the slowness.

In this example the physically relevant values for the reflection and transmission coefficients α^R, α^T at the wave speed interface are $\alpha^R = \dfrac{1}{16}, \alpha^T = \dfrac{15}{16}$. At $t = 1$, the exact density and averaged slowness are given by

$$\rho(x,1) = \begin{cases} 1, & -1.6 < x < -1.4; \\ 1+\alpha^R, & -1.4 < x < -0.4 - 1/3; \\ 1+\alpha^R + 0.6\alpha^T, & -0.4 - 1/3 < x < -0.4; \\ 1+\alpha^R + \alpha^T/0.6, & -0.4 < x < -0.2; \\ \alpha^T/0.3, & -0.2 < x < 0.2; \\ 1+\alpha^R + \alpha^T/0.6, & 0.2 < x < 0.4; \\ 1+\alpha^R + 0.6\alpha^T, & 0.4 < x < 0.4 + 1/3; \\ 1+\alpha^R, & 0.4 + 1/3 < x < 1.4; \\ 1, & 1.4 < x < 1.6; \end{cases} \tag{5.9}$$

and

$$u(x,1) = \frac{1}{\rho(x,1)} \begin{cases} 0.5, & -1.6 < x < -1.4; \\ 0.5 - \alpha^R \Upsilon(x+0.2), & -1.4 < x < -0.4 - \frac{1}{3}; \\ 0.5 - \alpha^R \Upsilon(x+0.2) - 0.36\alpha^T \Upsilon(0.6x - 1.16), & -0.4 - \frac{1}{3} < x < -0.6; \\ \Upsilon(x+0.6) - \alpha^R \Upsilon(x+0.2) - 0.36\alpha^T \Upsilon(0.6x - 1.16), & -0.6 < x < -0.4; \\ \frac{\alpha^T}{0.36}\Upsilon(\frac{x}{0.6} + \frac{13}{15}) - \Upsilon(x-1) + \alpha^R \Upsilon(x+1.8), & -0.4 < x < -0.2; \\ \frac{\alpha^T}{0.36}\Upsilon(\frac{x}{0.6} + \frac{13}{15}) - \frac{\alpha^T}{0.36}\Upsilon(\frac{x}{0.6} - \frac{13}{15}), & -0.2 < x < 0.2; \\ -\frac{\alpha^T}{0.36}\Upsilon(\frac{x}{0.6} - \frac{13}{15}) + \Upsilon(x+1) - \alpha^R \Upsilon(x-1.8), & 0.2 < x < 0.4; \\ -\Upsilon(x-0.6) + \alpha^R \Upsilon(x-0.2) + 0.36\alpha^T \Upsilon(0.6x + 1.16), & 0.4 < x < 0.6; \\ -0.5 + \alpha^R \Upsilon(x-0.2) + 0.36\alpha^T \Upsilon(0.6x + 1.16), & 0.6 < x < 0.4 + \frac{1}{3}; \\ -0.5 + \alpha^R \Upsilon(x-0.2), & 0.4 + \frac{1}{3} < x < 1.4; \\ -0.5, & 1.4 < x < 1.6; \end{cases} \tag{5.10}$$

with $\Upsilon(x) = 0.5 - \frac{0.4}{(1.6)^2}x^2$.

The time step is chosen as $\Delta t = \frac{1}{2}\Delta\xi$. Table 5.2 presents the l^1-error of numerical density ρ and averaged slowness u computed with several different meshes on the domain $[-1.6, 1.6] \times [-1.2, 1.2]$. It can be observed that the l^1-convergence rate of the numerical solutions is about 1/2 order.

Figure 5.4 shows the numerical solutions of density ρ and averaged slowness u using the 797×640 mesh along with the exact solutions. The numerical solution

Table 5.2 l^1 error of the numerical moments with different meshes

grid points	97×80	197×160	397×320	797×640
ρ	0.330508	0.224384	0.161847	0.114253
u	0.114813	0.084303	0.060016	0.042667

captures the correct dynamics and discontinuities. However, without a decomposition technique proposed in [20], the resolution is poorer than those in Example 5.1. Thus more efficient numerical methods needed to be developed in order to produce higher resolution solution for such measured-valued data.

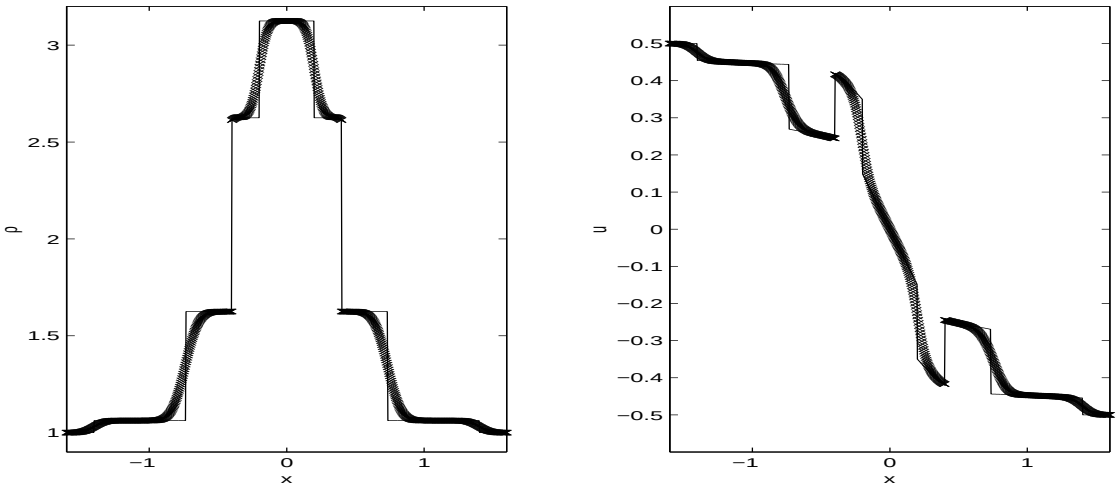

Figure 5.4 Example 5.2, density and averaged slowness in the physical space at $t = 1$. Solid line: the exact solution; 'x': numerical solutions using the 797×640 mesh. Left: density; Right: averaged slowness.

Example 5.3. Computing the physical observables of a 2D problem with a L^∞ solution. Consider the 2D Liouville equation (4.1) with a discontinuous wave speed

$$c(x,y) = \begin{cases} 2 & y > 0 \\ 1 & y < 0 \end{cases}$$

and a smooth initial data

$$f(x,y,\xi,\eta,0) = \frac{1}{\pi c_3 c_4}\exp\left(-\left(\frac{x}{c_1}\right)^2 - \left(\frac{y+0.1}{c_2}\right)^2 - \left(\frac{\xi}{c_3}\right)^2 - \left(\frac{\eta-0.1}{c_4}\right)^2\right)$$

where $c_1 = 0.03, c_3 = 0.05, c_2 = c_4 = 0.025$.

In this example we aim at computing the density which is the zeroth moment of the density distribution

$$\rho(x, y, t) = \int \int f(x, y, \xi, \eta, t) d\xi d\eta. \tag{5.11}$$

The computational domain is chosen to be $[x, y, \xi, \eta] \in [-0.12, 0.12] \times [-0.2, 0.2] \times [-0.2, 0.2] \times [-0.2, 0.2]$.

In this example the physically relevant values for the reflection and transmission coefficients α^R, α^T at the wave speed interface are given by (2.4). The exact phase space solution $f(x, y, \xi, \eta, t)$ can be obtained by the characteristic method, then we numerically compute the integral (5.11) on a fine mesh in (ξ, η) space. The results give very accurate density solution which is used as "exact" density solution to compare with the numerical densities computed by our finite difference scheme.

The time step is chosen as $\Delta t = \frac{1}{3}\Delta x$. Figures 5.5 and 5.7 show respectively the numerical density ρ at $t = 0.12, 0.15$ using different meshes along with the exact solution. Figure 5.6,5.8 show respectively the numerical density on $x = 0$ at $t = 0.12, 0.15$ using different meshes along with the exact solution.

Table 5.3 presents the l^1 errors of the numerical density ρ computed with different meshes in phase space at $t = 0.12, 0.15$. The convergence rate is slightly higher than first order, which does not suffer from the accuracy degeneration of usual finite difference method for solving the discontinuous solution of linear hyperbolic equation–which is at most 1/2 order stated by the well established theory [24], [35]. This is because the only discontinuity in the solutions is at the interface, and no linear discontinuity travels to the downstream direction like in the one-dimensional case, which has been take care of by the Hamiltonian-preserving mechanism.

Table 5.3 l^1 error of numerical density ρ using different meshes

grid points	$13 \times 20 \times 14^2$	$25 \times 40 \times 26^2$	$49 \times 80 \times 50^2$
$t = 0.12$	1.241556E-3	5.252852E-4	1.722251E-4
$t = 0.15$	1.244387E-3	6.621391E-4	2.617174E-4

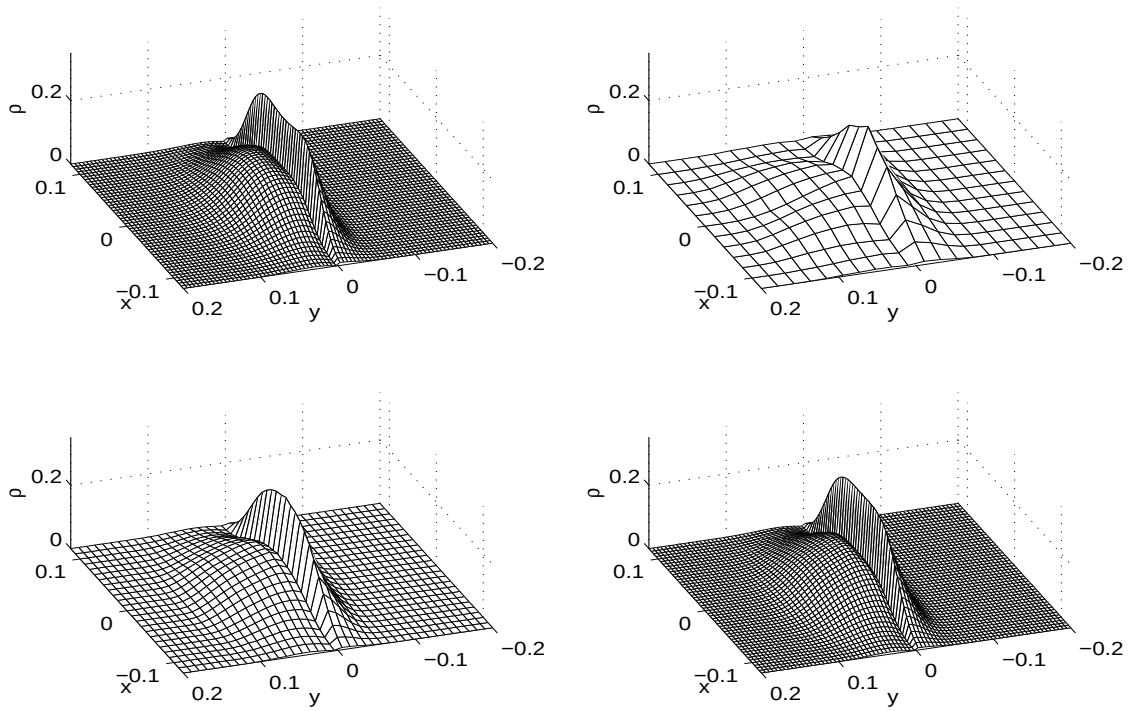

Figure 5.5 Example 5.3, density in the physical space at $t = 0.12$. Upper left: exact solution; Upper right: $13 \times 20 \times 14^2$ mesh; Lower left: $25 \times 40 \times 26^2$ mesh; Lower right: $49 \times 80 \times 50^2$ mesh.

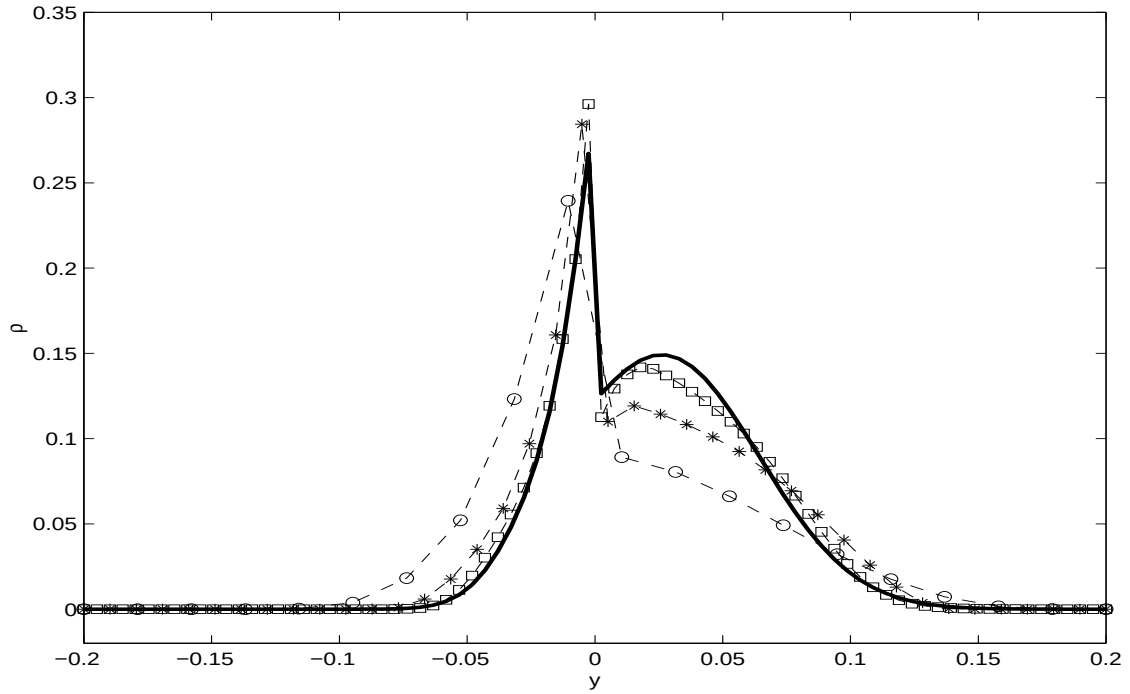

Figure 5.6 Example 5.3, density along $x = 0$ at $t = 0.12$. Solid line: exact solution; 'o': $13 \times 20 \times 14^2$ mesh; '*': $25 \times 40 \times 26^2$ mesh; '□': $49 \times 80 \times 50^2$ mesh.

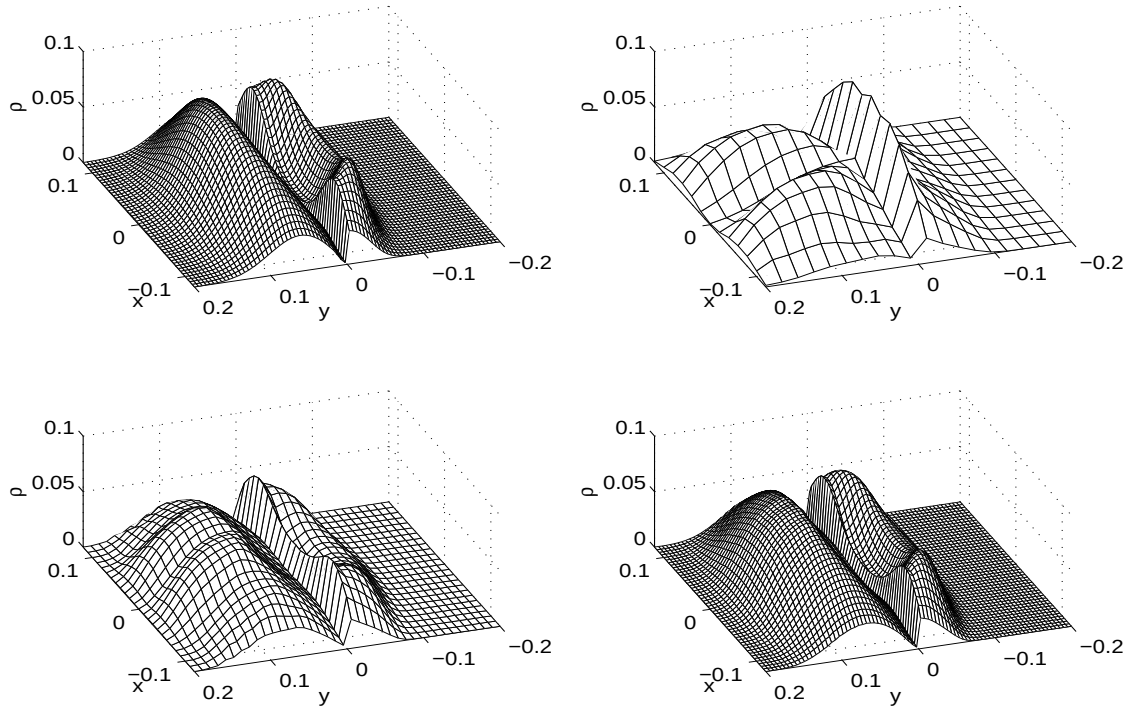

Figure 5.7 Example 5.3, density in the physical space at $t = 0.15$. Upper left: exact solution; Upper right: $13 \times 20 \times 14^2$ mesh; Lower left: $25 \times 40 \times 26^2$ mesh; Lower right: $49 \times 80 \times 50^2$ mesh.

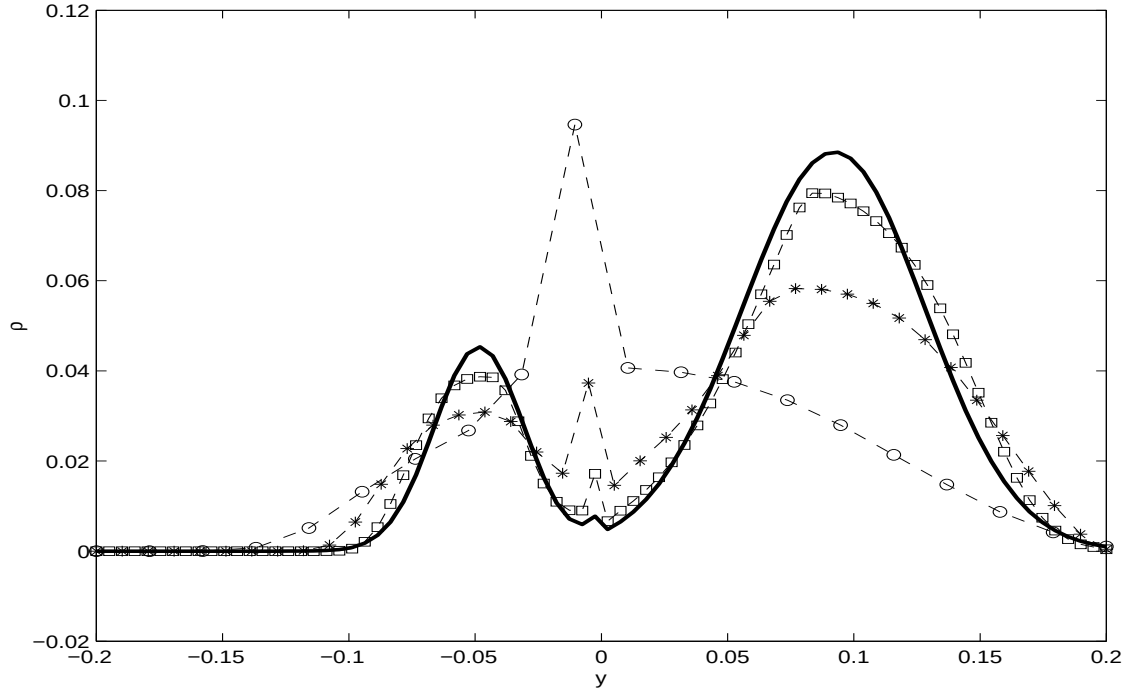

Figure 5.8 Example 5.3, density along $x = 0$ at $t = 0.15$. Solid line: exact solution; 'o': $13 \times 20 \times 14^2$ mesh; '*': $25 \times 40 \times 26^2$ mesh; '□': $49 \times 80 \times 50^2$ mesh.

6 Conclusion

In this paper, we extended our previous work [23] to the Liouville equation of geometrical optics to the general case of coexistence of transmissions and reflections. Such problems arise in geometrical optics with interfaces. While still utilizing the constant Hamiltonian structure in constructing the numerical flux, we also account for the transmission and reflection coefficients into the scheme. This allows an explicit scheme for time independent Liouville equation with discontinuous local wave speeds with a hyperbolic CFL condition, under which the scheme is positive, and stable in both l^1 and l^∞ norms. Numerical experiments are carried out to study the numerical accuracy.

We only extended a finite difference version of the Hamiltonian-preserving scheme developed in [23]. The finite volume version of the method in [23] can also be extended in a similar fashion, but will not be given here.

In the future we will consider more complex interfaces, and more effective methods for the measure-valued initial value problem for the same equation.

References

[1] G. Bal, J.B. Keller, G. Papanicolaou and L. Ryzhik, Transport theory for acoustic waves with reflection and transmission at interfaces, Wave Motion, 30, 303-327 (1999).

[2] J.-D. Benamou, Big Ray Tracing: Multivalued Travel Time Field Computation Using Viscosity Solutions of the Eikonal Equation, J. Comput. Phys. 128, 463-474 (1996).

[3] J.-D. Benamou, Direct computation of multivalued phase space solutions for Hamilton-Jacobi equations, Comm. Pure Appl. Math. 52(11), 1443-1475 (1999).

[4] J.-D. Benamou, An introduction to Eulerian geometrical optics(1992-2002), J. Sci. Comp. 19(1-3), 63-93, Dec. (2001).

[5] J.-D. Benamou and I. Solliec, An Eulerian Method for Capturing Caustics, J. Comput. Phys. 162(1), 132-163 (2000).

[6] F. Bouchut and F. James, One-dimensional transport equations with discontinuous coefficients, Nonlinear Analysis, Theory, Methods and Applications 32, 891-933, 1998.

[7] Li-Tien Cheng, Myungjoo Kang, Stanley Osher, Hyeseon Shim, and Yen-Hsi Tsai, Reflection in a Level Set Framework for Geometric Optics , Computer Modeling in Engineering and Sciences 5, 347-360, 2004.

[8] L.-T. Cheng, H.-L. Liu and S. Osher, Computational high-frequency wave propagation using the Level Set method, with applications to the semi-classical limit of Schrödinger equations, Comm. Math. Sci. 1, 593-621, 2003.

[9] B. Engquist and O. Runborg, Multi-phase computations in geometrical optics, J. Comput. Appl. Math. 74, 175-192 (1996).

[10] B. Engquist and O. Runborg, Multiphase computations in geometrical optics, In M. Fey and R. Jeltsch, editors, Hyperbolic Problems: Theory, Numerics, Applications, volume 129 of Internat. Ser. Numer. Math., Zürich, Switzerland, 1998. ETH Zentrum.

[11] B. Engquist and O. Runborg, Computational high frequency wave propagation, Acta Numerica 12, 181-266 (2003).

[12] B. Engquist, O. Runborg and A.-K. Tornberg, High-Frequency Wave Propagation by the Segment Projection Method, J. Comput. Phys. 178(2), 373-390 (2002).

[13] B. Engquist, A.K. Tornberg and R. Tsai, Discretization of dirac delta functions in level set methods, J. Comp. Phys., to appear.

[14] E. Fatemi, B. Engquist and S. Osher, Numerical solution of the high frequency asymptotic expansion for the scalar wave equation, J. Comput. Phys. 120, 145-155 (1995).

[15] S. Fomel and J.A. Sethian, Fast Phase Space Computation of Multiple Arrivals, Proc. Natl. Acad. Sci. USA 99(11), 7329-7334 (2002).

[16] L. Gosse, Using K-branch entropy solutions for multivalued geom etric optics computations, J. Comp. Phys. 180, 155–182, 2002.

[17] L. Gosse, Multiphase semiclassical approximation of an electron in a one-dimensional crystalline lattice II. Impurities, confinement and Bloch oscillations, J. Comp. Phys. 201, 344-375, 2004.

[18] L. Gosse, S. Jin and X.T. Li, On Two Moment Systems for Computing Multiphase Semiclassical Limits of the Schrodinger Equation Math. Model Methods Appl. Sci. 13, 1689-1723, 2003.

[19] S. Jin, H.L. Liu, S. Osher and R. Tsai, Computing multivalued physical observables for the semiclassical limit of the Schrodinger equation, J. Comp. Phys., in press.

[20] S. Jin, H.L. Liu, S. Osher and R. Tsai, Computing multi-valued physical observables for high frequency limit of symmetric hyperbolic systems, J. Comp. Phys., to appear.

[21] S. Jin and S. Osher, A level set method for the computation of multi-valued solutions to quasi-linear hyperbolic PDE's and Hamilton-Jacobi equations, Comm. Math. Sci. 1(3), 575-591 (2003).

[22] S. Jin and X. Wen, Hamiltonian-preserving schemes for the Liouville equation with discontinuous potentials, submitted to Communications in Mathematical Sciences.

[23] S. Jin and X. Wen, Hamiltonian-preserving schemes for the Liouville equation of geometrical optics with discontinuous local wave speeds, submitted to J. Comp. Phys.

[24] N.N. Kuznetsov, On stable methods for solving non-linear first order partial differential equations in the class of discontinuous functions, Topics in Numerical Analysis III (Proc. Roy. Irish Acad. Conf.)(J.J.H.Miller, ad.), Academic Press, London, 183-197 (1977).

[25] R.J. LeVeque, Numerical Methods for Conservation Laws, Birkhauser-Verlag, Basel, 1990.

[26] L. Miller, Refraction of high frequency waves density by sharp interfaces and semiclassical measures at the boundary, J. Math. Pures Appl. IX 79, 227-269, (2000).

[27] S. Osher, L.-T. Cheng, M. Kang, H. Shim and Y.-H. Tsai, Geometric optics in a phase-space-based level set and Eulerian framework, J. Comput. Phys. 179(2), 622-648 (2002).

[28] B. Perthame and C.W. Shu, On positivity preserving finite volume schemes for Euler equations, Numer. Math. 73, 119-130 (1996).

[29] B. Perthame and C. Simeoni, A kinetic scheme for the Saint-Venant system with a source term, CALCOLO 38(4), 201-231 (2001).

[30] O. Runborg, Some new results in multiphase geometrical optics, M2AN Math. Model. Numer. Anal. 34, 1203-1231 (2000).

[31] L. Ryzhik, G. Papanicolaou and J. Keller, Transport equations for elastic and other waves in random media, Wave Motion 24, 327-370 DEC (1996).

[32] L. Ryzhik, G. Papanicolaou and J. Keller, Transport equations for waves in a half space, Comm. PDE's, 22, 1869-1910 (1997).

[33] C.W. Shu and S. Osher, Efficient implementation of essentially non-oscillatory shock capturing scheme, J. Comput. Phys. 77, 439-471 (1988).

[34] W. Symes and J. Qian, A slowness matching Eulerian method for multivalued solutions of Eikonal equations, J. Sci. Comp. 19(1-3), 501-526, (2003). Special issue in honor of the sixtieth birthday of Stanley Osher.

[35] T. Tang and Z.H. Teng, The sharpness of Kuznetsov's $O(\sqrt{\Delta x})$ L^1-error estimate for monotone difference schemes, Math. Comp. 64, 581-589 (1995).